Wide Design Range of Constant Output Current Using Double-Sided *LC* Compensation Circuits for Inductive-Power-Transfer Applications

Xiaohui Qu, *Member, IEEE*, Haijun Chu, Zhicong Huang, *Member, IEEE*, Siu-Chung Wong, *Senior Member, IEEE*, Chi K. Tse, *Fellow, IEEE*, Chunting Chris Mi, *Fellow, IEEE*, and Xi Chen, *Senior Member, IEEE*

***Abstract*—Inductive-power-transfer (IPT) converters should desirably achieve nearly zero reactive circulating power, soft switching of power devices and load-independent constant output voltage or current with optimized transfer efficiency, and lowest component ratings. However, the load-independent output characteristic is dependent on IPT transformer parameters and their compensation. The space-constrained IPT transformer restricts the design of the low-order resonant circuit compensated IPT converter, making the IPT converter hard to optimize. This paper will analyze conditions under which any extra design freedom can be allowed for a double-sided *LC* compensation circuit in order to achieve load-independent output and zero reactive power input. A detailed analysis is given for the double-sided *LC* compensation achieving zero reactive power input and constant current output, without being constrained by the transformer parameters. Design conditions of the compensation circuit parameters for achieving these two properties are derived. A complementary *LC-CC* compensated IPT converter is further proposed to extend the output current amplitude limitation of the double-sided *LC* compensated IPT converter. Finally, the prototypes of the IPT converters are constructed to verify the design flexibility of the proposed double-sided *LC* compensation circuit for achieving the multiple objectives.**

***Index Terms*—Design flexibility, double-sided *LC* compensation, inductive power transfer (IPT), power converter.**

Manuscript received January 3, 2018; revised March 18, 2018; accepted May 17, 2018. Date of publication May 22, 2018; date of current version February 5, 2019. This work was supported in part by the National Natural Science Foundation of China (51677027), in part by the Fundamental Research Funds for Central Universities of China, and in part by the Hong Kong RGC General Research Fund (PolyU 152082/17E). Recommended for publication by Associate Editor C. T. Rim. *(Corresponding author: Xiaohui Qu.)*

X. Qu and H. Chu are with the School of Electrical Engineering, Southeast University, Nanjing 210096, China (e-mail: xhqu@seu.edu.cn; chuhaij@163.com).

Z. Huang, S.-C. Wong, and C. K. Tse are with the Department of Electronic and Information Engineering, The Hong Kong Polytechnic University, Hong Kong (e-mail: forward.huang@gmail.com; enscwong@polyu.edu.hk; encktse@polyu.edu.hk).

C. C. Mi is with the Department of Electrical and Computer Engineering, San Diego State University, San Diego, CA 92182 USA (e-mail: mi@ieee.org).

X. Chen is with the GEIRI North America, San Jose, CA 95134 USA (e-mail: xc@ieee.org).

Color versions of one or more of the figures in this paper are available online at http://ieeexplore.ieee.org.

Digital Object Identifier 10.1109/TPEL.2018.2839769

I. Introduction

RECENTLY, inductive power transfer (IPT) has drawn significant attentions due to its unique advantages in practical applications, such as wireless charging of electric vehicles [1]–[3], consumer electronics [4], LED lighting applications [5]–[7], biomedical implants [8], [9], etc. The transmitter and receiver in an IPT system are the primary winding and secondary winding of the loosely coupled transformer, which has a relatively large amount of uncoupled magnetic flux fleeing into the air. It is well known that the output power can be dramatically maximized by using the resonant transmitter and receiver at the same resonant frequency. Thus, the resonant circuits, formed by the IPT transformer and external passive inductors or capacitors, are crucial in the IPT converter and also named as compensation circuits. As a resonant converter, the IPT converter has complex characteristics of output power, input impedance, efficiency, and so on, all of which may involve transformer coupling and load variation.

Controllable output power and maximum transfer efficiency are the uppermost objectives for all IPT power applications. Resonant inductive coupling has a higher power output compared with nonresonant inductive coupling with the same component ratings. Well-designed compensation circuits facilitate the realization of resonant inductive coupling with zero reactive circulating power driven by the IPT inverter. The output load only contributes as a damper to the resonant networks and thus, the resonant frequency is usually independent of load variation. Generally, IPT applications can be classified as stationary or dynamic, depending on a stable or a variable transformer coupling. Even in stationary IPT applications, any misalignment or gap variation can induce variation of coupling within an IPT transformer. Coupling variation always exists in dynamic IPT applications and may lead to the severe power null phenomenon. Much research has focused on the optimization of coupler design to improve the coupling tolerance, or relied on control methodology to cope with the variable resonant frequency. For example, the double-D quadrature pad [10], [11], bipolar pad [12], and polyphase structure [13], [14] are proposed to reduce the transformer parameter variation to an acceptable level. As a result, the transferred power and efficiency can be kept within the required limits. Variable frequency control can be performed

to keep the converter resonance with varying transformer coupling [15], [16]. Alternatively, operating at a fixed operating frequency, variable inductors [17] and switching capacitors [18] are usually used to keep the IPT converter perfectly tuned. In this way, considering the load variation, an additional front–end regulator or a downstream converter is needed to regulate the output power. However, it will challenge the design of the front–end or the downstream converter due to the large output fluctuation of the unregulated IPT converter when its load is varying.

It is reported that the maximum available efficiency of a loosely coupled transformer only depends on the coupling coefficient and quality factors of windings [19], [20]. Prior research has designed the coupler with high coupling coefficients, such as double-D pad [19], [21], and to use high-quality litz wires to reduce losses. Further efficiency improvement of an IPT converter includes the realization of soft switching of the high-frequency inverters and the optimal load matching during operation. A slight inductive input impedance for the zero-voltage switching (ZVS) turning-ON of MOSFETs and a slight capacitive input impedance for the zero-current switching turning-OFF of Insulated Gate Bipolar Transistor (IGBTs) are expected. If the compensation circuits facilitate the IPT converter having nearly resistive input impedance, nearly zero reactive power and soft switching can be achieved simultaneously by a slight tuning of the input impedance. In most applications, the load varies in a wide range. The optimal load for maximum efficiency is related to the IPT transformer design [7]. If the optimal load is designed within a desired load range, the single-stage IPT converter can guarantee operating at high efficiencies.

As a summary, compensation circuits could help the IPT converter to have the following desirable characteristics.

1) *Maximum output power and minimum volt–ampere (VA) ratings*. The primary and secondary compensation circuits are both resonating at the operating frequency. Proper compensation can make the input impedance resistive to minimize the component VA ratings and eliminate the reactive power stress on the inverter circuit.
2) *Maximum transfer efficiency*. Soft switching of power MOSFETs or IGBTs in the IPT converter could further increase efficiency. A slight inductive or capacitive input impedance can be readily obtained by a small twist of a component value from the compensation circuit tuned from the purely resistive input impedance point.
3) *Design achievable for any desired load-independent constant output regardless of the IPT transformer being optimized to meet the requirement of some physical dimensions.* The compensation circuit provides an extra flexibility on designing at the required output voltage or current without any extra power converter. Moreover, the output can be further designed to be load-independent. These characteristics will simplify the control and achieve a single-stage design.

However, it can be difficult for a compensation circuit in an IPT converter to fulfill all the above characteristics within a load range.

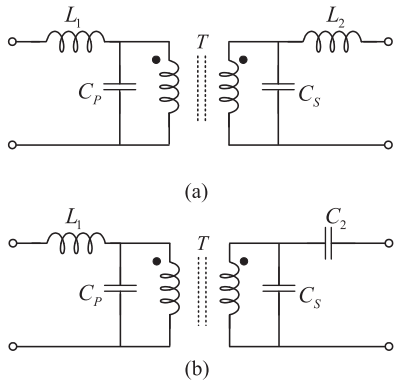

Fig. 1. Compensation circuits. (a) With double-sided *LC* topology. (b) With double-sided *LC-CC* topology.

Four basic types of compensation networks have been investigated with some desired properties at certain specified operating frequencies [22], [23]. For example, at the input zero-phase angle (ZPA) frequency, series–series (SS), and parallel–parallel (PP) compensation networks can realize a load-independent constant output current, whereas series-parallel (SP) and parallel-series (PS) compensation can realize a load-independent constant output voltage. However, the load-independent constant output current or voltage of IPT converters using any of these four compensation networks is greatly affected by the transformer parameters. In many IPT applications, the size and location of the loosely coupled transformer are often restricted and the available transformer parameters may not be able to achieve the requirement of constant output current or voltage. To solve this problem, higher order compensation networks with more compensation components and hence more design freedom are introduced [24]–[29]. In [24], the compensation circuits with one capacitor on one side and a T or Π network on the other side, show good performance in combating the transformer parameter constraints. Moreover, nearly zero reactive power and soft switching can be achieved simultaneously. More design freedom certainly facilitates the IPT converter design.

In [24], the primary and secondary compensation circuits having four external compensating components can realize load-independent constant output current or voltage at a load-independent ZPA frequency. There are other reported compensation circuits using more components, such as *LCC–LCC* with six external inductors and capacitors at two sides of the transformer [25]–[27]. Although more compensation components can increase the freedom of design, it is more complex to tune all the components appropriately for the desired performance, and then the cost and size of the IPT system will also increase. It is desirable to meet the design requirements using a minimum number of components. The double-sided *LC* compensation circuit, also called *LCL–LCL* topology, as shown in Fig. 1(a), appears in many applications, especially in bidirectional IPT applications due to the symmetrical structure [28], [29]. It also has four external compensating components, and more design freedom is expected for combating the constraints

of the transformer. However, this double-sided *LC* topology is usually designed with a symmetry between the primary and secondary circuitries, including the transformer self-inductances and the external compensation components. Moreover, the output of the existing design of a double-sided *LC* compensation or *LCC–LCC* compensation is still constrained by the transformer parameters. In some applications, such as EV charging, the primary winding underneath the ground is usually much larger than the secondary winding placed underneath the car. Besides, the IPT converter using the compensation circuits in [24] has the unique ZPA frequency for either load-independent constant current output or constant voltage output. The *LCC–LCC* compensated IPT converter has at least two ZPA frequencies for both load-independent constant current and constant voltage outputs, which is very suitable for lithium battery charging [30]. However, the characteristics of load-independent output, input ZPA, and soft switching of the double-sided *LC* compensated IPT converter are rarely studied systematically. To solve the issues, this paper will give a detailed analysis of the double-sided *LC* compensated IPT converter and prove that the ZPA frequencies only exist for load-independent constant current output and there is no ZPA frequency for load-independent constant voltage output. Given a set of IPT transformer parameters and an input dc voltage, a design procedure will be proposed to achieve the load-independent constant output current, nearly zero reactive power and soft switching for IPT converters. A limitation on the output current amplitudes of the double-sided *LC* compensated IPT converter will be reported. An asymmetric *LC-CC* topology will then be proposed as a complementary topology of the double-sided *LC* topology, as shown in Fig. 1(b), to extend the limit of the output amplitude of the double-sided *LC* compensation circuit. The two complementary topologies can realize the whole range of load-independent constant output while input ZPA and soft switching can also be realized. The sensitivities of transfer function and input impedance to variation of the compensation parameters, and their effects on achieving soft switching and the required constant output will be discussed. Finally, prototypes of the IPT converters will be built to verify the design flexibility of using a single-IPT transformer and the two compensation circuits for achieving the constant output current.

Specifically, Section II introduces the characteristics of the double-sided *LC* compensation circuit that facilitate the load-independent output, input ZPA, and soft switching. Parameter design and limitation are also analyzed and a new *LC-CC* compensation circuit is proposed for further analysis. Section III gives the design consideration of the IPT converters using these two compensation circuits. The performance of these two converters are evaluated in Section IV. Finally, Section V concludes this paper.

II. Characteristics of Double-Sided *LC* Compensation Circuits

To facilitate the analysis, the IPT converter using a double-sided *LC* compensation circuit is driven by a purely sinusoidal ac voltage source $v_{\rm IN}$ with an angular frequency ω, and delivers power to an equivalent load R_E, as shown in Fig. 2. The loosely coupled transformer is modeled as a three-parameter *T* network, where L_P and L_S are the self-inductances of the primary side and secondary side, respectively, and M is the mutual inductance. The transformer is compensated by external elements L_1, L_2, C_P, and C_S. Essential currents $i_{\rm IN}$, i_P, i_S, and i_r are shown in Fig. 2.

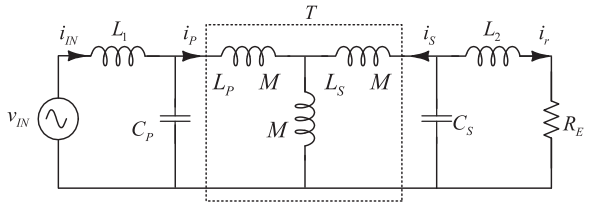

Fig. 2. Schematic of the IPT converter using the double-sided *LC* compensation.

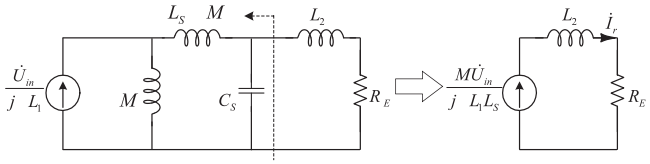

Fig. 3. Derivation of the IPT converter using the double-sided *LC* compensation.

A. Realization of Input ZPA and Load-Independent Constant Output

To obtain the characteristic of load-independent constant output current or voltage, circuit simplification by using Thevénin's and Norton's theorems at local resonance is performed. From Fig. 2, input voltage source $v_{\rm IN}$ cascading with L_1 and C_P is simplified to an ideal phasor current source $\frac{\dot{U}_{\rm in}}{j\omega L_1}$, as shown in Fig. 3, where L_1 and C_P satisfy

$$\omega = \frac{1}{\sqrt{L_1 C_P}} \tag{1}$$

and $\dot{U}_{\rm in}$, $\dot{I}_{\rm in}$, $\dot{I}_P$, $\dot{I}_S$, and $\dot{I}_r$ are phasors of $v_{\rm IN}$, $i_{\rm IN}$, i_P, i_S, and i_r, respectively. Similarly, Fig. 3 can be further simplified by first transforming the parallel connection of $\frac{\dot{U}_{\rm in}}{j\omega L_1}$ and M to a series connection of voltage source $\frac{\dot{U}_{\rm in} M}{L_1}$ and an inductor M. The overall series connected $\frac{\dot{U}_{\rm in} M}{L_1}$, M, $L_S - M$, and C_S are combined and transformed to the Norton form, as shown in the right-hand side of Fig. 3, with L_S and C_S forming a resonant tank, giving

$$\omega = \frac{1}{\sqrt{L_S C_S}} \tag{2}$$

where the transconductance of the IPT converter is given as

$$G = \frac{\dot{I}_r}{\dot{U}_{\rm in}} = \frac{M}{j\omega L_S L_1}. \tag{3}$$

Obviously, the output current is independent of the load and determined by the transformer parameters and the additional external inductor L_1. With a predesigned transformer, the extra

design freedom given by L_1 can flexibly generate a constant output current.

Fig. 4 shows an IPT converter using an equivalent two-port transformer *M* model. Define $Z_S = j\omega L_S + \frac{1}{j\omega C_S} \| (j\omega L_S + R_E)$ as the secondary equivalent impedance. From the secondary side of Fig. 4, we obtain

$$j\omega M \dot{I}_P = -\dot{I}_S Z_S. \tag{4}$$

Replacing the primary dependent source as an equivalent impedance $Z_R = \frac{j\omega M \dot{I}_S}{\dot{I}_P}$ and substituting Z_R into (4), we obtain $Z_R = \frac{\omega^2 M^2}{Z_S}$. The input impedance can be written as

$$Z_{\rm IN} = j\omega L_1 + \frac{1}{j\omega C_P} \| (j\omega L_P + Z_R). \tag{5}$$

The requirement of the ZPA is equivalent to $\Im(Z_{\rm IN}) = 0$, which gives

$$L_2 = \frac{L_S}{L_P k^2} \left[L_1 - L_P (1 - k^2) \right] \tag{6}$$

where k is the transformer coupling coefficient given by $k = \frac{M}{\sqrt{L_P L_S}}$.

From (3), L_1 is determined by the required output current amplitude. From (6), the actual behavior of inductor L_2 depends on the values of L_1 and $L_P(1 - k^2)$. Thus, the following three conditions are considered here.

1) If $L_1 > L_P(1 - k^2)$, L_2 is an inductor with value given by (6). Especially, if L_1 is designed as L_P, L_2 equals L_S.
2) If $L_1 = L_P(1 - k^2)$, $L_2 = 0$. The double-sided *LC* topology becomes the traditional PP compensation structure. The transconductance G of a PP structure is $\frac{M}{j\omega(L_S L_P - M^2)}$, which is dependent upon the transformer parameters [23].
3) If $L_1 < L_P(1 - k^2)$, $L_2 < 0$ and it should practically be a capacitor C_2, resulting in an asymmetric *LC-CC* structure, as shown in Fig. 1(b). Accordingly, we have $X_{\rm L2} = X_{\rm C2}$, which gives

$$C_2 = \frac{C_S L_P k^2}{L_P(1 - k^2) - L_1}. \tag{7}$$

In summary, load-independent output current and input ZPA require L_1 to satisfy (3), and L_2 or C_2 to satisfy (6) or (7). The operating angular frequency ω_0 of $v_{\rm IN}$ is set to ω. Compensation capacitors C_P and C_S are calculated using (1) and (2).

B. Other Frequencies for Input ZPA and Load-Independent Constant Output

Section II-A shows that there exists an operating frequency ω_0 at which input ZPA and load-independent output current can be achieved for the IPT converter. With the parameters mentioned, it is useful to find out whether there are other frequencies at which input ZPA and load-independent output current or voltage can be achieved. Assume that there is another operating frequency $\omega_{\rm CC} = \alpha_{\rm CC}\omega_0$ at which load-independent current output is achieved. At $\omega_{\rm CC}$, Fig. 2 is transformed to Fig. 5 by Norton's theorem, where the input voltage source connected in series with L_1 and C_P becomes a phasor current $\frac{\dot{U}_{\rm in}}{j\omega_{\rm CC} L_1}$ paralleled with an equivalent inductor $\frac{L_1}{1-\alpha_{\rm CC}^2}$. Combining with transformer parameters $L_P - M$ and M, the circuit can be further transformed to a current source $\dot{I}_1$ and a parallel-connected inductor $L_{\rm eq}$, as shown in the right-hand side of Fig. 5. To achieve constant output current, inductor $L_{\rm eq}$ in series with $L_S - M$ should be at resonance with C_S. Thus, we have

$$L_{\rm eq} = M - \frac{M^2}{\frac{L_1}{1-\alpha_{\rm CC}^2} + L_P} \text{ and} \tag{8}$$

$$L_{\rm eq} + L_S - M = \frac{1}{\omega_{\rm CC}^2 C_S}. \tag{9}$$

Substituting (8) into (9), the value of coefficient $\alpha_{\rm CC}$ for load-independent constant output current is calculated as

$$\alpha_{\rm CC} = \sqrt{\frac{L_1 + L_P}{L_P(1 - k^2)}}. \tag{10}$$

Transconductance $G_{\rm CC}$ at $\omega_{\rm CC}$ is given by

$$G_{\rm CC} = \frac{\dot{I}_r}{\dot{U}_{\rm in}} = \frac{1}{j\omega_{\rm CC}} \cdot \frac{M}{L_1 L_S + L_P L_S (1 - k^2)(1 - \alpha_{\rm CC}^2)}. \tag{11}$$

Similarly, define another input ZPA frequency $\omega_{\rm ZPA} = \alpha\omega_0$. Then, $\Im(Z_{\rm IN}(\omega_{\rm ZPA})) = 0$. Assume that $Z_{\rm IN}$ in (5) can be written in the form of $\frac{A + Bj}{C + Dj}$. Solving for variables A, B, C, and D, we have (12). At the ZPA frequency $\omega_{\rm ZPA}$, we have $BC - AD = 0$. Substituting (12) into equation $BC - AD = 0$ and assuming that $L_1 \neq L_P$, there is only one solution for $\omega_{\rm ZPA}$ with $\alpha = 1$, i.e., $\omega_{\rm ZPA} = \omega_0$. Although there are two load-independent constant-current frequencies ω_0 and $\omega_{\rm CC}$, only ω_0 can realize the input ZPA. However, if $L_1 = L_P$, equation $BC - AD = 0$ has two solutions. One solution is $\alpha = 1$ and the other is $\alpha = \sqrt{\frac{2}{1-k^2}}$. Here, $\omega_{\rm ZPA} = \omega_0 \sqrt{\frac{2}{1-k^2}}$ is exactly $\omega_{\rm CC}$ at $L_1 = L_P$. Thus, if $L_1 = L_P$, there are two ZPA frequencies ω_0 and $\omega_0 \sqrt{\frac{2}{1-k^2}}$ to realize load-independent constant output current.

For load-independent constant output voltage, the operating frequencies can be derived by repeating the above steps using Thevénin circuit simplification. The detailed derivation is omitted here. Because the ZPA frequencies match the operating frequencies for constant output current well, there is definitely no frequency satisfying both input ZPA and constant output voltage. Therefore, the IPT converters based on double-sided *LC* compensation or *LC-CC* compensation can only provide constant output current with the lowest ratings of power switches, which is suitable for loads requiring a driving current, e.g., LEDs in lighting or batteries in charging application.

C. Bidirectional Operation for Both Compensation Circuits

Double-sided *LC* compensated IPT converter is widely used in the bidirectional applications due to the symmetrical structure. Although the extended *LC-CC* compensation circuit is asymmetrical for some output current range, it is important to explore the possibility of bidirectional operation for these two compensation circuits with the parameters given in Section II-A.

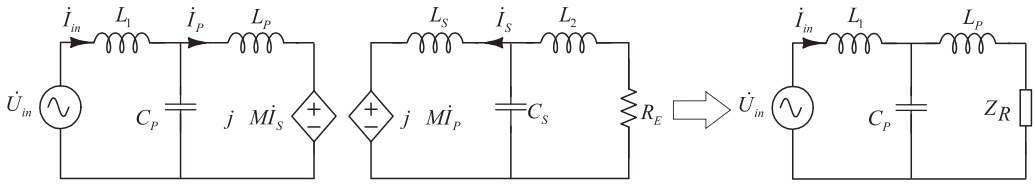

Fig. 4. IPT converter in Fig. 2 using a two-port transformer *M* model.

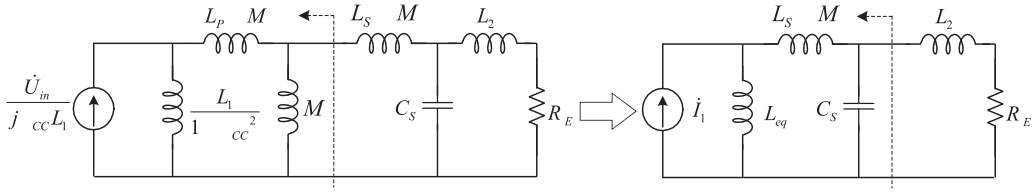

Fig. 5. Derivation of the IPT converter operating at another frequency ω_{CC} with load-independent constant output current.

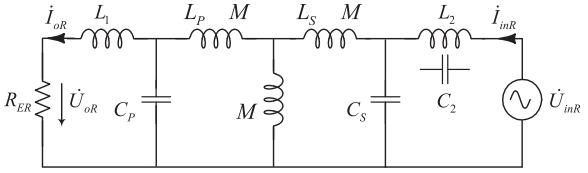

Fig. 6. Double-sided *LC* or *LC-CC* compensation in reverse operation.

The IPT converter in Fig. 2 can be modeled as a two-port network with the matrix A, which is given by

$$\begin{bmatrix} \dot{U}_{\mathrm{in}} \\ \dot{I}_{\mathrm{in}} \end{bmatrix} = A \begin{bmatrix} \dot{U}_r \\ \dot{I}_r \end{bmatrix} = \begin{bmatrix} 0 & \frac{M}{j\omega L_S L_1} \\ -\frac{M}{j\omega L_S L_1} & 0 \end{bmatrix} \begin{bmatrix} \dot{U}_r \\ -\dot{I}_r \end{bmatrix}. \quad (13)$$

Here, $\dot{U}_r$ is the phasor voltage of R_E. In the reverse operation, as shown in Fig. 6, (13) becomes

$$\begin{bmatrix} \dot{U}_{\mathrm{oR}} \\ -\dot{I}_{\mathrm{oR}} \end{bmatrix} = A \begin{bmatrix} \dot{U}_{\mathrm{inR}} \\ -\dot{I}_{\mathrm{inR}} \end{bmatrix}. \quad (14)$$

Rearranging (14), it gives

$$\begin{aligned} \begin{bmatrix} \dot{U}_{\mathrm{inR}} \\ -\dot{I}_{\mathrm{inR}} \end{bmatrix} &= A^{-1} \begin{bmatrix} \dot{U}_{\mathrm{oR}} \\ -\dot{I}_{\mathrm{oR}} \end{bmatrix} \\ &= \begin{bmatrix} 0 & -\frac{j\omega L_S L_1}{M} \\ -\frac{j\omega L_S L_1}{M} & 0 \end{bmatrix} \begin{bmatrix} \dot{U}_{\mathrm{oR}} \\ -\dot{I}_{\mathrm{oR}} \end{bmatrix}. \end{aligned} \quad (15)$$

For both *LC-LC* and *LC-CC* compensation circuits, the reverse operation still has the load-independent constant current, where the transconductance in the reverse operation is given as

$$G_R = \frac{\dot{I}_{\mathrm{oR}}}{\dot{U}_{\mathrm{inR}}} = \frac{M}{j\omega L_S L_1}. \quad (16)$$

Substituting $\dot{U}_{\mathrm{oR}} = \dot{I}_{\mathrm{oR}} R_{\mathrm{ER}}$ into (15), the reverse input impedance Z_{INR} can be expressed as $Z_{\mathrm{INR}} = \frac{\dot{U}_{\mathrm{inR}}}{\dot{I}_{\mathrm{inR}}} = R_{\mathrm{ER}}$, which is purely resistive. Thus, both double-sided *LC* and *LC-CC* compensated converters can operate reversely with the characteristics of input ZPA and load-independent constant output current.

$$\begin{cases} A = \alpha^2\omega_0^2 L_P L_S \left[\left(k^2 - 1 - \left(\frac{L_1}{L_P} - 1 \right) \left(\frac{1}{k^2} - 1 \right) \right) \alpha^4 + \left(4 - 2k^2 + \frac{1}{k^2} \left(\frac{L_1}{L_P} - 1 \right) \left(\frac{L_1}{L_P} + 2 \right) \right) \alpha^2 + k^2 - 2 - \frac{2L_1}{L_P} \right. \\ \qquad \left. - \frac{1}{k^2} \left(\frac{L_1}{L_P} - 1 \right) \left(\frac{L_1}{L_P} + 1 \right) \right] \\ B = \alpha\omega_0 L_P R_E \left[(1 - k^2)\alpha^4 + \left(k^2 - 2 - \frac{L_1}{L_P} \right) \alpha^2 + 1 + \frac{L_1}{L_P} \right] \\ C = R_E \left[\frac{L_P}{L_1}(1 - k^2)\alpha^4 - \left(1 + \frac{L_P}{L_1} \right) \alpha^2 + 1 \right] \\ D = \alpha\omega_0 L_S \frac{L_P}{L_1} \left[\left(2 - k^2 - \frac{L_1}{L_P} + \frac{1}{k^2} \left(\frac{L_1}{L_P} - 1 \right) \right) \alpha^4 + \left(k^2 - 2 - \frac{L_1}{L_P} - \frac{1}{k^2} \left(\frac{L_1}{L_P} + 1 \right) \left(\frac{L_1}{L_P} - 1 \right) \right) \alpha^2 + \frac{2L_1}{L_P} \right. \\ \qquad \left. + \frac{1}{k^2} \frac{L_1}{L_P} \left(\frac{L_1}{L_P} - 1 \right) \right]. \end{cases} \quad (12)$$

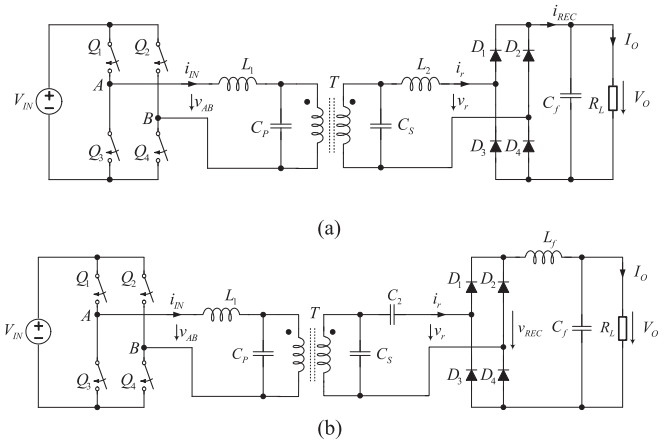

Fig. 7. Two IPT converters. (a) Using double-sided *LC* compensation. (b) Using double-sided *LC-CC* compensation.

III. Design and Implementation of the Two IPT Converters

As analyzed in Section II, depending on the required transconductance given by (3), and the relationship between L_1 and $L_P(1-k^2)$, the two IPT converters using double-sided *LC* and *LC-CC* compensation circuits as shown in Fig. 7 can be designed. At angular frequency ω_0, input ZPA and load-independent constant output current can be achieved. In practice, the full-bridge switches $Q_{1,2,3,4}$ operate at $\omega_0 = \frac{1}{\sqrt{L_1 C_P}} = \frac{1}{\sqrt{L_S C_S}}$ to generate a square voltage $v_{\rm AB}$. Here, the input dc voltage $V_{\rm IN}$ can be modulated by $Q_{1,2,3,4}$ with D being the duty cycle of $v_{\rm AB}$. The fundamental component of $v_{\rm AB}$, denoted as $v_{\rm IN}$, is given as

$$v_{\rm IN}(t) = \frac{4V_{\rm IN}}{\pi} \sin\frac{\pi D}{2} \sin(\omega_0 t + \theta). \tag{17}$$

A full-bridge diode rectifier and one capacitor filter, i.e., *C* filter, are used to rectify the ac output current and filter the ripple voltage before connecting to the output load, as shown in the Fig. 7(a). The ac output current turns ON the diodes of the rectifier bridge that follows the current path. The voltage waveform v_r before the rectifier becomes a square wave with voltage approximately equal to V_O. In Fig. 7(b), the voltages across C_2 and C_S cannot change suddenly to comply with the square wave voltage. Therefore, the *C* filter is not applicable here and an *LC* filter with one inductor and one capacitor is used to absorb the voltage fluctuation. The type of filters used determines the waveforms of the input and output of the rectifier, as shown in Fig. 8. The secondary current $i_r(t)$ equals $\frac{v_{\rm IN}(t)M}{\omega_0 L_S L_1}$ from (3). For the *C* filter, after the rectification, the equivalent output current is given as

$$I_{O_C} = \frac{2I_{\rm rpeak}}{\pi} = \frac{8}{\pi^2} \cdot \frac{V_{\rm IN} \sin\frac{\pi D}{2} M}{\omega_0 L_S L_1}. \tag{18}$$

For the *LC* filter

$$I_{O_{\rm LC}} = \frac{\pi I_{\rm rpeak}}{4} = \frac{V_{\rm IN} \sin\frac{\pi D}{2} M}{\omega_0 L_S L_1}. \tag{19}$$

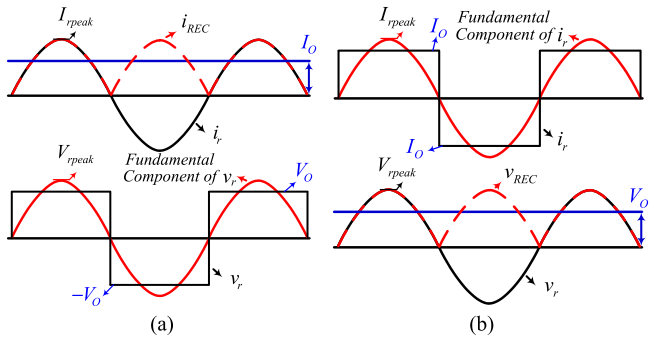

Fig. 8. Waveforms before and after the IPT secondary rectifier. (a) Using *C* filter. (b) Using *LC* filter.

For the IPT converter design with the required output current I_O, the given input dc voltage $V_{\rm IN}$ and transformer parameters, L_1 can be calculated by (18) or (19). The choice of the double-sided *LC* or *LC-CC* compensation depends on the relationship of L_1 and the transformer parameter $L_P(1-k^2)$. A summary is given as follows.

1) If $I_O < \frac{8V_{\rm IN}\sin\frac{\pi D}{2}M}{\pi^2\omega_0(L_P L_S - M^2)}$, i.e., $L_1 > L_P(1-k^2)$, a converter with the double-sided *LC* compensation and the corresponding output filter shown in Fig. 7(a) is used.
2) If $I_O > \frac{V_{\rm IN}\sin\frac{\pi D}{2}M}{\omega_0(L_P L_S - M^2)}$, i.e., $L_1 < L_P(1-k^2)$, a converter with the *LC-CC* compensation and the corresponding output filter shown in Fig. 7(b) is used.
3) If $\frac{8V_{\rm IN}\sin\frac{\pi D}{2}M}{\pi^2\omega_0(L_P L_S - M^2)} \le I_O \le \frac{V_{\rm IN}\sin\frac{\pi D}{2}M}{\omega_0(L_P L_S - M^2)}$, the converter with the *LC-CC* compensation and the corresponding output filter, as shown in Fig. 7(b), is used. Here, choose $L_1 < L_P(1-k^2)$ and adjust the duty cycle D as D', guaranteeing the required $I_O > \frac{V_{\rm IN}\sin\frac{\pi D'}{2}M}{\omega_0(L_P L_S - M^2)}$, i.e., $\sin\frac{\pi D'}{2} \le \frac{8}{\pi^2}\sin\frac{\pi D}{2}$.

With the chosen *LC–LC* or *LC-CC* topology and operating frequency ω_0, C_P from (1), C_S from (2), L_2 or C_2 from (6) or (7) can be uniquely calculated. In this way, the ZPA between $v_{\rm AB}$ and $i_{\rm IN}$ can be guaranteed. To permit the ZVS of MOSFETs $Q_{1,2,3,4}$, the input impedance should be slightly inductive. A slight increment or decrement of L_1, C_P, C_S, L_2, or C_2 can fulfill the requirement. However, the small variation or tolerance in these components may also affect the output current accuracy. Hence, the sensitivity of parameters should be against variation of the converter transconductance. If some variations of compensating parameter occur, the operating angular frequency ω may not satisfy (1) and (2) simultaneously. As a result, the load-independent constant output current in (3) will be unavailable. The input impedance and output current can be derived from Fig. 2 using the modified parameters $x_1 L_1$, $x_2 L_2$, $x_P C_P$, and $x_S C_S$ in (20), where x_1, x_2, x_P, and x_S denote normalized variation factors of L_1, L_2, C_P, and C_S, respectively.

The normalized output current can be given as $\left|\frac{I_r(x_1,x_2,x_P,x_S)}{I_r(1,1,1,1)}\right|$. For an *LC-CC* topology, $\frac{1}{j\omega x_2 C_2}$ can be used in (20) to replace $j\omega x_2 L_2$. Fig. 9 shows the normalized output current versus various normalized parameters, where variations of L_1 and L_2 or C_2 are clearly not sensitive to output current. Specifically, the variation of L_2 or C_2 does not affect the

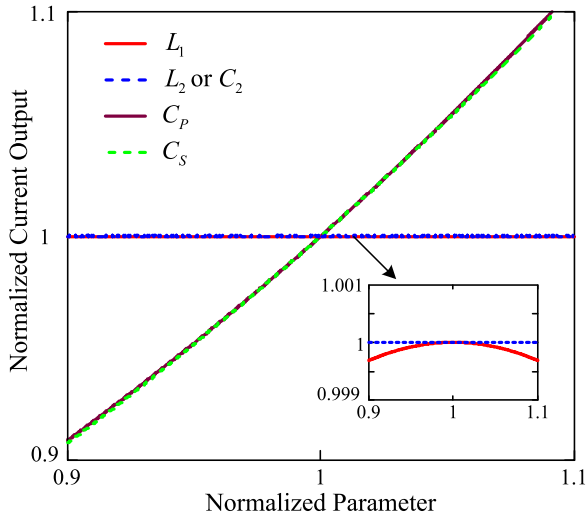

Fig. 9. Normalized current output with varying normalized parameters L_1, L_2 or C_2, C_P, and C_S.

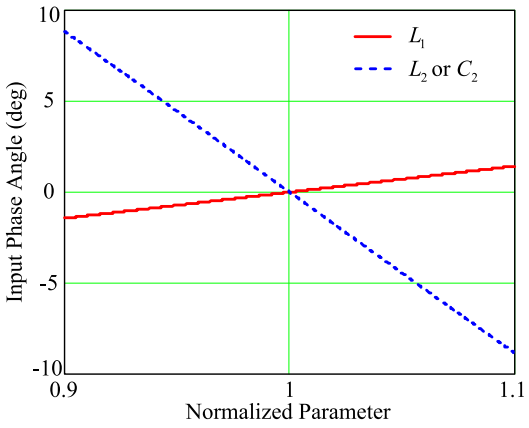

Fig. 10. Phase angle of input impedance versus variation of L_1 and L_2 or C_2.

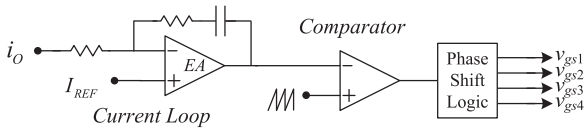

Fig. 11. Control schematic of both double-sided *LC* and *LC-CC* compensated IPT converters.

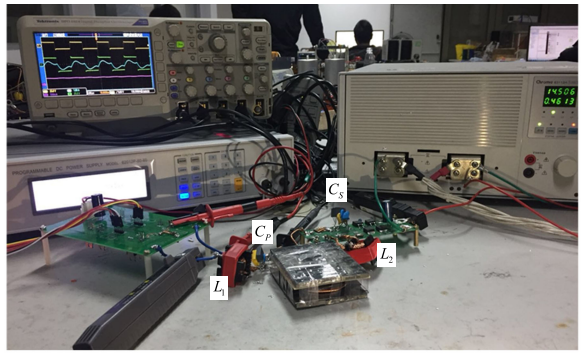

(a)

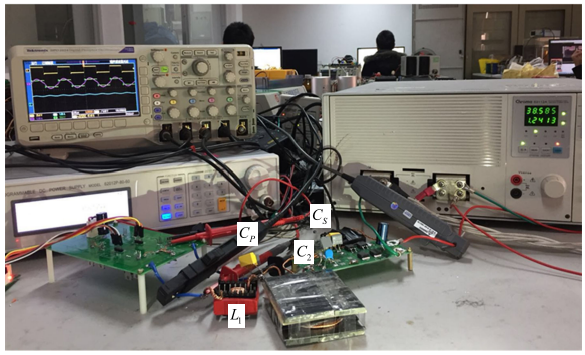

(b)

Fig. 12. Photographs of experimental setups. (a) With double-sided *LC* compensated IPT converter. (b) With double-sided *LC-CC* compensated IPT converter.

output current, which is consistent with the derivation shown in Fig. 4. The phase angle between the input voltage and current can be expressed as $\angle Z_{\rm IN}(x_1, x_2, x_P, x_S)$. Fig. 10 shows that a small increment of L_1 and a small decrement of L_2 or C_2 can be used to realize ZVS with negligible transconductance variation. Then, the usual fixed-frequency phase-shift control, as shown in Fig. 11, can be used to drive switches $Q_{1,2,3,4}$ for both double-sided *LC* and *LC-CC* compensated IPT converters. Any small variation of input voltage, transformer parameters, and compensation parameters will affect the output current. Here, the duty cycle control can compensate the effect of variations to output current until the output current equals the desired $I_{\rm REF}$.

IV. Experimental Evaluation

To verify the design flexibility of the double-sided *LC* and *LC-CC* compensated IPT converters, prototypes with a maximum power of up to 50 W using these two compensation

$$Z_{\rm IN}(x_1,x_2,x_P,x_S) = j\omega x_1 L_1 + \frac{1}{j\omega x_P C_P} \| \left\{ j\omega(L_P - M) + j\omega M \| \left[j\omega(L_S - M) + \frac{1}{j\omega x_S C_S} \| (j\omega x_2 L_2 + R_E) \right] \right\} \text{ and}$$

$$\dot{I}_r(x_1,x_2,x_P,x_S) = \frac{\dot{U}_{\rm in}}{Z_{\rm IN}(x_1,x_2,x_P,x_S)} \cdot \frac{\frac{1}{j\omega x_P C_P}}{\frac{1}{j\omega x_P C_P} + j\omega(L_P - M) + j\omega M \| \left[j\omega(L_S - M) + \frac{1}{j\omega x_S C_S} \| (j\omega x_2 L_2 + R_E) \right]}$$

$$\cdot \frac{j\omega M}{j\omega L_S + \frac{1}{j\omega x_S C_S} \| (j\omega x_2 L_2 + R_E)} \cdot \frac{\frac{1}{j\omega x_S C_S}}{\frac{1}{j\omega x_S C_S} + j\omega x_2 L_2 + R_E} \tag{20}$$

TABLE I
CALCULATED AND EXPERIMENTAL PARAMETERS IN COMPENSATION NETWORKS

Constant current	Compensation	Calculated				Experimental			
		L_1	C_P	C_S	L_2 or C_2	L_1	C_P	C_S	L_2 or C_2
0.28 A	LC-LC	37.17 μH	17.04 nF		56.50 μH	37.17μH	17.05 nF		55.95μH
0.46 A	LC-LC	22.63 μH	27.99 nF	26.71 nF	24.51 μH	22.33 μH	28.8 nF	26.8 nF	23.48 μH
1.28 A	LC-CC	10.03 μH	62.08 nF		225.6 nF	10.2 μH	62.42 nF		199 nF

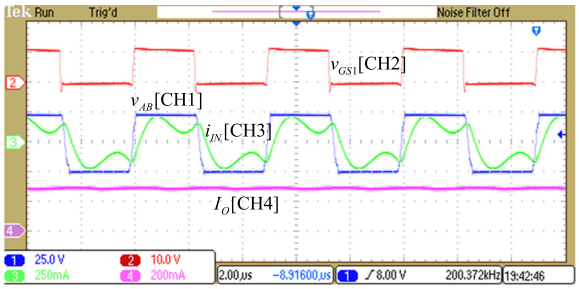

(a)

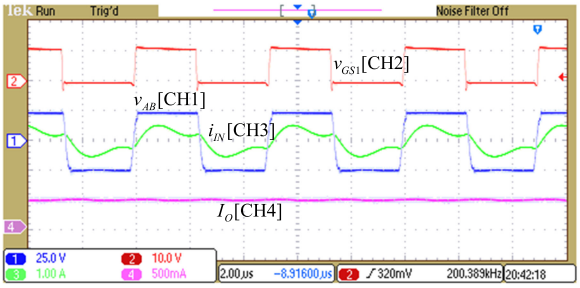

(b)

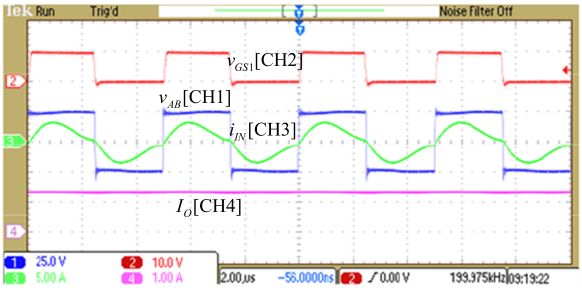

(c)

Fig. 13. Experimental waveforms of $v_{\rm GS1}$, $v_{\rm AB}$, $i_{\rm IN}$, and I_O with the same load of 30 Ω and different values of output current. (a) Double-sided *LC* compensation with $I_O =$ 0.28 A. (b) Double-sided *LC* compensation with $I_O =$ 0.46 A. (c) Double-sided *LC-CC* compensation with $I_O =$ 1.28 A.

configurations have been built to provide constant currents of 0.28, 0.46, and 1.28 A, where Fig. 12(a) shows the double-sided LC based IPT converter and Fig. 12(b) shows the *LC-CC*-based IPT converter. A single loosely coupled transformer is used in these three cases with $L_P = 22.26$ μH, $L_S = 23.71$ μH, and $M = 15.99$ μH. The test conditions are: $V_{\rm IN} = 24$ V, duty cycle D is 0.95, operating frequency $f_{\rm sw}$ is 200 kHz, and the desired values of I_O are 0.28 and 0.46 A. The converters use the double-sided *LC* compensation circuit satisfying the inequality $I_O < \frac{8V_{\rm IN}\sin\frac{\pi D}{2}M}{\pi^2\omega(L_P L_S - M^2)}$. For the case of $I_O = 1.28$ A, the converter uses the *LC-CC* compensation circuit satisfying the inequality $I_O > \frac{V_{\rm IN}\sin\frac{\pi D}{2}M}{\omega(L_P L_S - M^2)}$. The calculated and experimental parameters in these two compensation circuits are listed in Table I. From the sensitivity analysis of these components, the experimental values of L_1, C_P, and C_S are consistent with the calculated results for the required constant output current. The experimental value of L_2 or C_2 is chosen to be a little smaller than the calculated value for the realization of ZVS. The output filter uses L_f of 56 μH and C_f of 220 μF. A phase shift controller is used here with fixed frequency duty cycle control and then a feedback controller using UCC3895 is applied. Switches $Q_{1,2,3,4}$ are IRF540 and secondary rectifier diodes are MBRB20150CT.

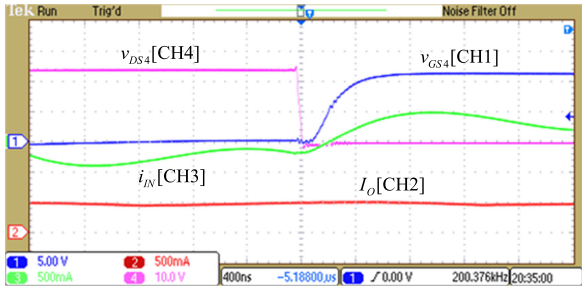

Fig. 14. Enlarged waveforms of $v_{\rm GS4}$, $v_{\rm DS4}$, $i_{\rm IN}$, and I_O at $I_O = 0.46$ A with the load of 20 Ω, showing ZVS of switches.

Fig. 13 (a)–(c) shows the measured waveforms of gate drive voltage $v_{\rm GS1}$, modulated voltage $v_{\rm AB}$, input current $i_{\rm IN}$, and output current I_O, for three different output currents 0.28, 0.46, and 1.28 A all with load resistance of 30 Ω. With the same IPT transformer, two different selected compensation circuits with three sets of parameters, as listed in Table I, are used to generate the required constant output current. Moreover, $i_{\rm IN}$ in each case is nearly in phase with $v_{\rm AB}$, verifying that the compensation circuit eliminates the most reactive power. The small phase angle of $i_{\rm IN}$ lagging $v_{\rm AB}$ facilitates the ZVS of the full-bridge switches. The enlarged turn-ON waveforms of Q_4 in the lagging leg at $I_O = 0.46$ A with load resistance of 20 Ω clearly verify the ZVS condition of all the switches, as shown in Fig. 14. To show the load-independent constant output current, Fig. 15 gives the transient waveforms of $v_{\rm GS1}$, V_O, and I_O at $I_O = 0.46$ A, with the load stepping from 40 to 20 Ω. After the closed-loop control is applied, the output current remains the same for two different loads. The other constant current cases have the same property and are not shown here. The efficiency at the maximum 50-W output and I_O of 1.28 A is measured as 92.4% using the Yokogawa WT1800E power analyzer, as shown in Fig. 16. The efficiency optimization is not the key objective of this paper and is omitted here.

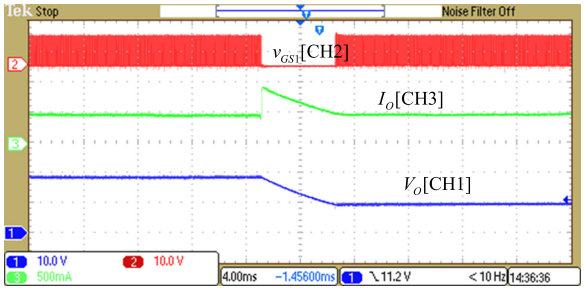

Fig. 15. Experimental waveforms of v_{GS1}, V_O, and I_O at $I_O = 0.46$ A in response to a step load from 40 to 20 Ω.

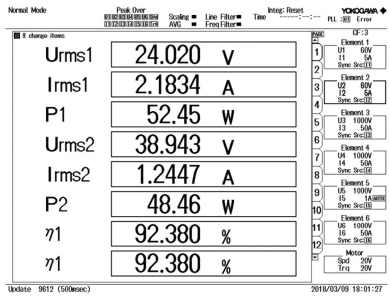

Fig. 16. Measured efficiency at $I_O = 1.28$ A and the output power of about 50 W. Here, U_{rms1}, I_{rms1}, and P_1 are the rms values of input dc voltage, input current, and input power, respectively, whereas U_{rms2}, I_{rms2}, and P_2 are the rms values of output voltage, output current I_O, and output power, respectively. I_{rms2} of 1.2447 A is a little lower than the required I_O of 1.28 A due to the line loss.

V. Conclusion

The space-constrained loosely coupled transformer poses a challenge to the design and optimization of the IPT converter. The double-sided *LC* compensation with four additional components has the design freedom to realize load-independent constant output current and input ZPA simultaneously. The desired output can be designed with different compensation parameters without the need to redesign the IPT transformer. The converter transfer function for the double-sided *LC* compensated IPT converter is analyzed and a new *LC-CC* compensated IPT converter is presented to extend the operating range of the converter. Moreover, the sensitivity of the converter transfer function against the variation of compensation components is analyzed. It is found that nearly zero reactive power stresses and soft switching of the power switches with high output current accuracy can be maintained over a wide operating range. The characteristic of load-independent output permits the implementation of simple fixed-frequency control.

References

[1] G. A. Covic and J. T. Boys, "Inductive power transfer," *Proc. IEEE*, vol. 101, no. 6, pp. 1276–1289, Jun. 2013.
[2] W. Y. Lee, J. Huh, and S. Y. Choi, "Finite-width magnetic mirror models of mono and dual coils for wireless electric vehicles," *IEEE Trans. Power Electron.* , vol. 28, no. 13, pp. 1413–1428, Mar. 2013.
[3] Z. Li. C. Zhu, J. Jiang, K. Song, and G. Wei, "A 3-kW wireless power transfer system for sightseeing car supercapacitor charge," *IEEE Trans. Power Electron.*, vol. 32, no. 5, pp. 3301–3316, May 2017.
[4] S. Y. Hui, "Planar wireless charging technology for portable electronic products and Qi," *Proc. IEEE*, vol. 101, no. 6, pp. 1290–1301, Jun. 2013.
[5] H. H. Wu, J. Boys, G. Covic, and D. Robertson, "A practical 1.2 kW inductive power transfer lighting system using AC processing controllers," in *Proc. IEEE Conf. Ind. Electron. Appl.*, 2011, pp. 345–350.
[6] J. E. James, A. Chu, A. Sabitov, D. Robertson, and G. Covic, "A series tuned light power IPT stage lighting controller," in *Proc. IEEE Energy Conv. Congr. Expo.* , 2011, pp. 2843–2849.
[7] X. Qu, W. Zhang, S. C. Wong, and C. K. Tse, "Design of a current-source-output inductive power transfer LED lighting system," *IEEE J. Emerg. Sel. Topics Power Electron.*, vol. 3, no. 1, pp. 306–314, Mar. 2015.
[8] C. Chen, S. C. Wong, C. K. Tse, and X. Ruan, "Analysis, design, and control of a transcutaneous power regulator for artificial hearts," *IEEE Trans. Biomed. Circuits Syst.*, vol. 3, no. 1, pp. 23–31, Feb. 2009.
[9] D. Ahn and S. Hong, "Wireless power transmission with self-regulated output voltage for biomedical implant," *IEEE Trans. Ind. Electron.*, vol. 61, no. 5, pp. 2225–2235, May 2014.
[10] M. Budhia, J. T. Boys, G. A. Covic, and C. Y. Huang, "Development of a single-sided flux magnetic coupler for electric vehicle IPT charging systems," *IEEE Trans. Ind. Electron.*, vol. 60, no. 1, pp. 318–328, Jan. 2013.
[11] G. R. Nagendra, G. A. Covic, and J. T. Boys, "Sizing of inductive power pads for dynamic charging of EVs on IPT highways," *IEEE Trans. Transp. Electrific.*, vol. 3, no. 2, pp. 405–417, Jun. 2017.
[12] A. Zaheer, H. Hao, G. A. Covic, and D. Kacprzak, "Investigation of multiple decoupled coil primary pad topologies in lumped IPT systems for interoperable electric vehicle charging," *IEEE Trans. Power Electron.,* vol. 30, no. 4, pp. 1937–1955, Apr. 2015.
[13] X. Liu and S. Y. R. Hui, "Equivalent circuit modeling of a multilayer planar winding array structure for use in universal contactless battery charging platform," *IEEE Trans. Power Electron.,* vol. 22, no. 1, pp. 21–29, Jan. 2007.
[14] J. Achterberg, E. A. Lomonova, and J. de Boeij, "Coil array structures compared for contactless battery charging platform," *IEEE Trans. Magn.,* vol. 44, no. 5, pp. 617–622, May 2008.
[15] G. Xu, Q. Chen, X. Ren, S. C. Wong, and C. K. Tse, "Self-oscillating resonant converter with contactless power transfer and integrated current sensing transformer," *IEEE Trans. Power Electron.*, vol. 32, no. 6, pp. 4839–4851, Jun. 2017.
[16] E. Gati, G. Kampitsis, and S. Manias, "Variable frequency controller for inductive power transfer in dynamic conditions," *IEEE Trans. Power Electron.* , vol. 32, no. 2, pp. 1684–1696, Feb. 2017.
[17] N. Keeling, G. A. Covic, F. Hao, L. George, and J. T. Boys, "Variable tuning in LCL compensated contactless power transfer pickups," *Proc. IEEE Energy Convers. Congr. Expo.*, 2009, pp. 1826–1832.
[18] A. Kamineni, G. A. Covic, and J. T. Boys, "Self-tuning power supply for inductive charging," *IEEE Trans. Power Electron.*, vol. 32, no. 5, pp. 3467–3479, May 2017.
[19] S. Li and C. C. Mi, "Wireless power transfer for electric vehicle applications," *IEEE J. Emerg. Sel. Topics Power Electron.*, vol. 3, no. 1, pp. 4–17, Mar. 2015.
[20] W. Zhang and C. C. Mi, "Compensation topologies of high-power wireless power transfer systems," *IEEE Trans. Veh. Technol.*, vol. 65, no. 6, pp. 4768–4778, Jun. 2016.
[21] W. Zhang, J. C. White, A. M. Abraham, and C. C. Mi, "Loosely coupled transformer structure and interoperability study for EV wireless charging systems," *IEEE Trans. Power Electron.,* vol. 30, no. 11, pp. 6356–6367, Nov. 2015.
[22] W. Zhang, S. C. Wong, C. K. Tse, and Q. Chen, "Load-independent duality of current and voltage outputs of a series or parallel compensated inductive power transfer converter with optimized efficiency," *IEEE J. Emerg. Sel. Topics Power Electron.,* vol. 3, no. 1, pp. 137–146, Mar. 2015.
[23] X. Qu, H. Han, S. C. Wong, and C. K. Tse, "Hybrid IPT topologies with constant-current or constant-voltage output for battery charing applications," *IEEE Trans. Power Electron.*, vol. 30, no. 11, pp. 6129–6337, Nov. 2015.
[24] X. Qu, Y. Jing, H. Han, S. C. Wong, and C. K. Tse, "Higher order compensation for inductive-power-transfer converters with constant voltage or constant-current output combating transformer parameter constraints," *IEEE Trans. Power Electron.*, vol. 32, no. 1, pp. 394–405, Jan. 2017.

[25] S. Li, W. Li, J. Deng, T. D. Nguyen, and C. Mi, "A double-sided LCC compensation network and its tuning method for wireless power transfer," *IEEE Trans. Veh. Technol.,* vol. 64, no. 6, pp. 2261–2273, Jun. 2015.
[26] H. Feng, T. Cai, S. Duan, J. Zhao, X. Zhang, and C. Chen, "An LCC-compensated resonant converter optimized for robust reaction to large coupling variation in dynamic wireless power transfer," *IEEE Trans. Ind. Electron.*, vol. 63, no. 10, pp. 6591–6601, Oct. 2016.
[27] T. Kan, T. D. Nguyen, J. C. White, R. K. Malhan, and C. Mi, "A new integration method for an electric vehicle wireless charging system using LCC compensation topology: analysis and design," *IEEE Trans. Power Electron.*, vol. 32, no. 2, pp. 1638–1650, Feb. 2017.
[28] U. K. Madawala and D. J. Thrimawithana, "A bidirectional inductive power interface for electric vehicles in V2G systems," *IEEE Trans. Ind. Electron.*, vol. 58, no. 10, pp. 4789–4796, Oct. 2011.
[29] M. J. Neath, A. K. Swain, U. K. Madawala, and D. J. Thrimawithana, "An optimal PID controller for a bidirectional inductive power transfer system using multiobjective genetic algorithm," *IEEE Trans. Power Electron.*, vol. 29, no. 3, pp. 1523–1531, Mar. 2014.
[30] V. B. Vu, D. H. Tran, and W. J. Choi, "Implementation of the constant current and constant voltage charge of inductive power transfer systems with the double-sided LCC compensation topology for electric vehicle battery charge applications," *IEEE Trans. Power Electron.*, to be published.

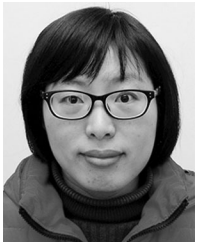

Xiaohui Qu (S'08–M'10) received the B.Eng. and M.Eng. degrees in electrical engineering from the Nanjing University of Aeronautics and Astronautics, Nanjing, China, in 2003 and 2006, respectively, and the Ph.D. degree in power electronics from The Hong Kong Polytechnic University, Hong Kong, in 2010.

From February to May 2009, she was engaged as a Visiting Scholar with the Center for Power Electronics Systems, Virginia Tech, Blacksburg, VA, USA. Since April 2010, she has been with the School of Electrical Engineering, Southeast University, China, as an Associate Professor with research focus on power electronics. From January 2015 to January 2016, she was a Visiting Scholar with the Center of Reliable Power Electronics, Aalborg University, Denmark. Her current research interests include LED lighting systems, wireless power transfer, and power electronics reliability.

Haijun Chu received the B.Eng. degree in electrical engineering from the Nanjing Institute of Technology, Nanjing, China, in 2016. He is currently working toward the M.Eng. degree in electrical engineering at Southeast University, Nanjing, China.

His current research interest mainly includes wireless power transfer.

Zhicong Huang (S'14–M'17) received the B.Eng. degree in electrical engineering and automation, in 2010, and the M.Eng. degree in mechanical and electronic engineering, in 2013, both from the Huazhong University of Science and Technology, Wuhan, China, and the Ph.D. degree in power electronics, in 2017, from The Hong Kong Polytechnic University, Hong Kong.

He currently holds a postdoctoral position with The Hong Kong Polytechnic University. His current research interests include wireless power transfer and smart energy conversion.

Siu-Chung Wong (M'01–SM'09) received the B.Sc. degree in physics from the University of Hong Kong, Hong Kong, in 1986, the M.Phil. degree in electronics from the Chinese University of Hong Kong, Hong Kong, in 1989, and the Ph.D. degree from the University of Southampton, Southampton, U.K., in 1997.

He was with The Hong Kong Polytechnic University, in 1988, as an Assistant Lecturer. He is currently an Associate Professor with the Department of Electronic and Information Engineering, The Hong Kong Polytechnic University, Hong Kong, where he conducts research in power electronics. He was a Visiting Scholar with the Center for Power Electronics Systems, Virginia Tech, VA, USA, in November 2008, Aero-Power Sci-Tech Center, Nanjing University of Aeronautics and Astronautics, Nanjing, China, in January 2009, and School of Electrical Engineering, Southeast University, Nanjing, China in March 2012.

Dr. Wong is a member of the Electrical College, The Institution of Engineers, Australia. He is an Associate Editor for the IEEE TRANSACTIONS ON CIRCUITS AND SYSTEMS II, an Editor for the *Energy and Power Engineering Journal* and a member of the Editorial Board of the *Journal of Electrical and Control Engineering*. In 2012, he was appointed as a Chutian Scholar Chair Professor by the Hubei Provincial Department of Education, China and the appointment was hosted by Wuhan University of Science and Technology, Wuhan, China. In 2013, he was appointed as a Guest Professor by the School of Electrical Engineering, Southeast University, Nanjing, China.

Chi K. Tse (M'90–SM'97–F'06) received the B.Eng. degree with first class Honors in electrical engineering and the Ph.D. degree from the University of Melbourne, Melbourne, VIC, Australia, in 1987 and 1991, respectively.

He is currently the Chair Professor with The Hong Kong Polytechnic University, Hong Kong, with which he served as the Head of the Department of Electronic and Information Engineering, from 2005 to 2012. His research interests include power electronics, nonlinear systems, and complex network applications.

Dr. Tse was a recipient of number of research and industry awards, including Prize Paper Awards by the IEEE Transactions on Power Electronics in 2001 and 2015, RISP Journal of Signal Processing Best Paper Award in 2014, Best paper Award by the International Journal of Circuit Theory and Applications in 2003, two Gold Medals at the International Inventions Exhibition in Geneva in 2009 and 2013, a Silver Medal at the International Invention Innovation Competition in Canada in 2016, and a number of recognitions by the academic and research communities, including honorary professorship by several Chinese and Australian universities, Chang Jiang Scholar Chair Professorship, IEEE Distinguished Lectureship, Distinguished Research Fellowship by the University of Calgary, Gledden Fellowship and International Distinguished Professorship-at-Large by the University of Western Australia. He serves and has served as an Editor-in-Chief for the IEEE TRANSACTIONS ON CIRCUITS AND SYSTEMS II (2016–2019), the IEEE CIRCUITS AND SYSTEMS MAGAZINE (2012–2015), an Editor-in-Chief for the IEEE Circuits and Systems Society Newsletter (since 2007), an Associate Editor for three IEEE Journal/Transactions, an Editor for the *International Journal of Circuit Theory and Applications*, and is on the editorial boards of a few other journals. He currently chairs the steering committee for the IEEE TRANSACTIONS ON NETWORK SCIENCE AND ENGINEERING. He also serves as a panel member for the Hong Kong Research Grants Council, and a member of several professional and government committees.

Chunting Chris Mi (S'00–A'01–M'01–SM'03–F'12) received the B.S.E.E. and M.S.E.E. degrees in electrical engineering from Northwestern Polytechnical University, Xian, China, in 1985 and 1988, respectively, and the Ph.D. degree in electrical engineering from the University of Toronto, Toronto, ON, Canada, in 2001.

He is currently a Professor and the Chair of electrical and computer engineering and the Director of the Department of Energy-funded Graduate Automotive Technology Education Center for Electric Drive Transportation, San Diego State University (SDSU), San Diego, CA, USA. Prior to joining SDSU, he was with the University of Michigan, Dearborn, MI, USA, from 2001 to 2015. He was the President and the Chief Technical Officer of 1Power Solutions, Inc., from 2008 to 2011. He is the Cofounder of Gannon Motors and Controls LLC and Mia Motors, Inc. He has conducted extensive research and has authored/coauthored more than 100 journal papers. He has taught tutorials and seminars on the subject of HEVs/PHEVs for the Society of Automotive Engineers (SAE), the IEEE, workshops sponsored by the National Science Foundation, and the National Society of Professional Engineers. He has delivered courses to major automotive OEMs and suppliers, including GM, Ford, Chrysler, Honda, Hyundai, Tyco Electronics, A & D Technology, Johnson Controls, Quantum Technology, Delphi, and the European Ph.D. School. He has offered tutorials in many countries, including USA, China, Korea, Singapore, Italy, France, and Mexico. He has published more than 100 articles and delivered 30 invited talks and keynote speeches. His research interests include electric drives, power electronics, electric machines, renewable-energy systems, and electrical and hybrid vehicles.

Dr. Mi was a recipient of the Distinguished Teaching Award, the Distinguished Research Award of University of Michigan, Dearborn, the 2007 IEEE Region 4 Outstanding Engineer Award, the IEEE Southeastern Michigan Section Outstanding Professional Award, and the SAE Environmental Excellence in Transportation. He has also served as a Panelist in major IEEE and SAE conferences.

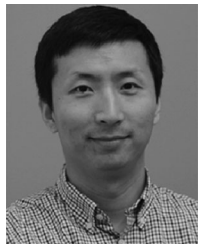

Xi Chen (S'07–M'13–SM'16) received the M.Sc. and Ph.D. degrees from the King's College London, University of London, London, U.K., and The Hong Kong Polytechnic University, Hong Kong, in 2005 and 2009, respectively.

From 2009 to 2011, he was with the Center of Internet of Things Research and Development, State Grid Information and Telecommunication Company, Ltd., Beijing, China, as a Research Fellow. He was a Postdoctoral Research Fellow with the Institute of Software, Chinese Academy of Science, Beijing, China, from 2011 to 2013. In 2014, he joined the GEIRI North America, San Jose, CA, USA, where he is currently the Director of development and planning. His research interests include smart grid, electric vehicle charging infrastructure, Internet of Things, and complex networks analysis and its applications.